A NUMERICAL STUDY OF CONSTRAINT AND RATE EFFECTS ON DYNAMIC CRACK GROWTH

Xi Zhang[1] and Yiu-Wing Mai[2,3]

[1] CSIRO Division of Petroleum Resources, PO Box 3000, Glen Waverley, VIC 3150, Australia
[2] Centre for Advanced Materials Technology (CAMT), School of Aerospace, Mechanical and Mechatronic Engineering J07, The University of Sydney, Sydney, NSW 2006, Australia
[3] MEEM, City University of Hong Kong, Tat Chee Avenue, Kowloon, Hong Kong

ABSTRACT

A transient finite element analysis has been carried out to provide insight into the dynamic crack growth behavior in viscoplastic materials under plane strain and small-scale yielding conditions. The fracture process is characterized by an embedded cohesive zone model in which the macroscopic fracture work is a function of crack opening rate and temperature rise on the crack flanks. The material is an isotropic hardening and thermal softening elastic-plastic von Mises solid. The computational model is developed to identify the individual roles of crack-tip constraint, loading rates and cohesive law properties. There is a sharp rise in the fracture resistance curves after a small amount of crack growth. The competition of strain-rate hardening and thermal softening in the fracture process zone can significantly change the fracture resistance curves. The effects of loading rates and crack-tip constraints have been examined. It is shown that the trend of increasing toughness due to the negative T-stress is greatly reduced when crack growth is fully developed. In addition, crack-tip constraint does not affect the limiting crack speed.

KEYWORDS

Dynamic fracture; Rate effect; Thermal effect; Constraint; Embedded cohesive zone model

INTRODUCTION

One class of models that serves as a bridge between the macroscopic and microscopic methods is that of the embedded cohesive zone model (ECZM). The fracture process is represented in terms of a traction-separation relation applied on the plane of fracture, while the bulk materials are considered by conventional continuum mechanics. Although this model cannot directly account for the interaction of the crack tip and the voids nearest to it, the implication of all these factors can be qualitatively put into a phenomenological cohesive law through some primary parameters [1]. It is more flexible than the cell model and easier for implementation of finite element methods. In addition, ECZM provides an illustrating and tractable way to include constitutive non-linearity into the continuum models.

Fracture behavior depends strongly on loading rate, material response and finite geometry change.

Emphasis is placed on dynamic crack growth such that inertia effect becomes significant. The class of materials considered here is hardened by increasing effective plastic strain rate and weakened by temperature rise. It is inferred that fast crack growth will have lower toughness since the elevated traction acts on the plane of separation due to strain-rate hardening. However, the inconsistent trend found in recent experiments by Du *et al* [2] and theoretical analyses [3,4] showed that rate-dependent materials must have a rate-dependent fracture process.

The effect of crack-tip constraint on fracture toughness has attracted a great deal of interest during the past decade. For stationary cracks in some specimen geometries, there is loss of J-dominance of crack-tip fields due to the non-uniqueness of hydrostatic stress [5,6]. The same problem has been extended to quasi-static crack growth in ductile materials by Xia and Shih [7] using a cell model and by Tvergaard and Hutchinson [1] using a cohesive zone model. However, crack-tip constraint effects on the dynamic fracture process have not been fully exploited.

The objective of the present paper is to consider the influences of crack-tip constraint, material inertia and thermal softening on the crack growth resistance. To this end, finite element simulations of mode I plane strain crack growth under small-scale yielding conditions are carried out for a range of material parameters. A rate- and thermal-dependent traction-separation relation is used to model the fracture process. The material considered is an isotropic hardening and linear thermal softening viscoplastic solid.

CONSTITUTIVE EQUATIONS OF THE SOLID AND THE FRACTURE PROCESS

We adopt a thermal-viscoplastic constitutive relation with linear thermal softening and power-law strain-rate hardening. The deformation rate tensor is decomposed into elastic, viscoplastic and thermal parts:

$$\mathbf{D} = \mathbf{D}^{e} + \mathbf{D}^{vp} + \mathbf{D}^{T} \tag{1}$$

For an isotropic hardening, viscoplastic solid, the plastic part of the deformation-rate tensor and the thermal dilatation take the forms:

$$\mathbf{D}^{vp} = (\frac{3\dot{\bar{\varepsilon}}}{2\sigma_e})\mathbf{S} \qquad \mathbf{D}^{T} = \alpha\Delta\dot{T}\mathrm{I} \tag{2}$$

where $\dot{\bar{\varepsilon}}$ denotes the equivalent plastic strain rate, $\mathbf{S} = \mathbf{t} - 1/3\mathbf{t}\cdot\mathbf{I}$ the deviator of Kirchoff stress $\mathbf{t}$, and $\mathbf{s}_e = \sqrt{3\mathbf{S}:\mathbf{S}/2}$ the equivalent stress, α the thermal expansion coefficient, ΔT the temperature rise and $\mathbf{I}$ the second order identity tensor. The constitutive relation can be written as:

$$\overset{\nabla}{\mathbf{t}} = \mathbf{L}:[\mathbf{D} - \mathbf{D}^{vp} - \mathbf{D}^{T}] \tag{3}$$

where $\overset{\nabla}{\boldsymbol{t}}$ is the Jaumann rate of Kirchoff stress tensor, $\mathbf{L}$ is elastic modulus tensor with Young's modulus E and Possion's ratio ν. The effective plastic strain rate becomes:

$$\dot{\bar{\varepsilon}} = \dot{\bar{\varepsilon}}_0[\frac{\sigma_e}{g(\bar{\varepsilon},T)}]^{1/m}$$
$$g(\bar{\varepsilon},T) = \sigma_0(1+\bar{\varepsilon}/\varepsilon_0)^{N}[1-\beta(T-T_0)] \tag{4}$$

where $\bar{\varepsilon} = \int_0^t \dot{\bar{\varepsilon}}dt$ denotes the equivalent plastic strain, $\dot{\bar{\varepsilon}}_0$ is reference strain rate, m rate sensitivity parameter, σ_0 yield stress, $\varepsilon_0 = \sigma_0/E$ reference strain, N strain hardening exponent, T_0 reference temperature, usually equal to the environmental temperature, abd β thermal softening coefficient.

The form of the static traction-separation law given by Tvergaard and Hutchinson [1] is adopted here. The parameters characterizing the traction-separation curves include the work of fracture per

unit area, the peak stress for separation $\hat{\sigma}$ and three characteristic lengths, $\delta_1, \delta_2, \delta_c$. The shape parameters δ_1 and δ_2 are chosen so that $\delta_1 = 0.15\delta_c$ and $\delta_2 = 0.5\delta_c$. It is shown that these factors are of secondary importance in failure assessment [1]. The fracture work, $\Gamma_0 = \int_0^{\delta_c} \sigma(\delta, \dot{\delta}, T) d\delta = \hat{\sigma}(\delta_c + \delta_1 - \delta_2)/2$, is not a constant because of the effects of material inertia and thermal softening. Further, it is assumed that the rate and the thermal effects on the fracture work were incorporated into the model in terms of the changes in the peak traction $\hat{\sigma}$. The cohesive strength is written as:

$$\hat{\sigma} = \hat{\sigma}_0 (1 + \frac{\dot{\delta}}{\dot{\delta}_0})^{r_1} [1 - r_2 (T - T_0)] \tag{5}$$

where r_1 and r_2 are material constants which describe the rate effect and thermal softening, $\dot{\delta}_0$ (=1 m/s) is reference separation rate and $\hat{\sigma}_0$ is steady-state traction for the quasi-static cohesive zone model, and $T_0 = 20^0 C$.

COMPUTATIONAL MODEL

Finite element simulations described here are based on updated coordinate Lagrangian formulation. All physical quantities are functions of a set of moving coordinates x^i at time t. Consider an equilibrium crack in a body with current volume V, surface S_{ext} subjected to a velocity constraint and internal cohesive surface area S_{coh}. The weak form of the governing equations for mechanical fields yields the incremental form for the principle of virtual work on the current configuration [8]:

$$\int_V \tau^{ik} \delta D_{ij} dV - \int_{S_{coh}} S^i \delta \dot{u}_i dS = \int_{S_{ext}} T^i \delta \dot{u}_i dS - \int_V K^i \delta \dot{u}_i dV \tag{6}$$

where τ^{ij} are the Kirchoff stress tensor components equal to those of the Cauchy stress tensor σ^{ij} in the current configuration, $D_{ij} = (\dot{u}_{i,j} + \dot{u}_{j,i})/2$ are deformation rate tensor components and $\dot{u}_i$ are displacement rate vector components. The kinetic energy $K_i = 0.5\rho \partial^2 u_i / \partial t^2$ in which ρ is the mass density in the current configuration, T^i and S^i are the traction components on the external surface S_{ext} and internal cohesive surface S_{coh}. It should be noted that the Kirchoff stress is identical to the Cauchy stress if we take the current state as the reference configuration.

Also, the local balance of energy gives the following governing equation for the conduction of heat in a continuous medium:

$$\rho c_p \frac{\partial T}{\partial t} = \kappa T_{,ii} + \gamma w^p \tag{7}$$

where c_p is heat capacity, κ is thermal conductivity and the parameter γ specifies the fraction of plastic work ($w^p = \sigma^{ij} D_{ij}^p$) that is converted to heat and is taken to have a value 0.90.

The crack growth analyses are carried out under small-scale yielding conditions. Due to symmetry about the crack plane only half of the solid needs to be analyzed. A semi-circular region with initial radius R_0 = 20 mm is used in the numerical computation. It is chosen so that $R_0 = 2000\Delta$ where Δ is the size of the smallest elements of the mesh at the crack-tip. $\delta_c = 0.1\Delta$ is selected to determine the minimum dimension of these elements if they are not specified. The mesh consists of 1584×4 triangle elements and a uniform mesh region with an initial length $L_0 = 48\Delta$ is used to model crack growth. A length twice L_0 can be taken as the uniform mesh zone since the mesh size is increased at a ratio near unity from the minimum size.

On the outer semi-circular boundary, the displacements, $\dot{u}_1$ and $\dot{u}_2$, are given by the external stress fields, according to small strain linear elastic fracture mechanics solutions. Thus, we have

$$\dot{u}_1(x^1, x^2, t) = \frac{2(1+\nu)\dot{K}_I}{E}\sqrt{\frac{R_0}{2\pi}}\cos\frac{\theta}{2}(1-2\nu+\sin^2\frac{\theta}{2})$$
$$\dot{u}_2(x^1, x^2, t) = \frac{2(1+\nu)\dot{K}_I}{E}\sqrt{\frac{R_0}{2\pi}}\sin\frac{\theta}{2}(1-2\nu+\cos^2\frac{\theta}{2}) \quad (8)$$

in which $R_0 = \sqrt{x_1^2 + x_2^2}$, $\theta = \tan^{-1}(x^2/x^1)$ for the points on the remote boundary in the current configuration, and $\dot{K}_I$ measures the incremental rate of the mode I stress intensity factor.

To minimize the wave effect, the initial velocities throughout the region are given by [9]:

$$\dot{u}_1(x^1, x^2, 0) = \frac{2(1+\nu)\dot{K}_I}{E}\sqrt{\frac{r}{2\pi}}\cos\frac{\theta}{2}(1-2\nu+\sin^2\frac{\theta}{2})$$
$$\dot{u}_2(x^1, x^2, 0) = \frac{2(1+\nu)\dot{K}_I}{E}\sqrt{\frac{r}{2\pi}}\sin\frac{\theta}{2}(1-2\nu+\cos^2\frac{\theta}{2}) \quad (9)$$

in which $r = \sqrt{x_1^2 + x_2^2}$.

At t=0, the non-singular stress term, T-stress, is applied uniformly. In this work, the T-stress T is applied together with the corresponding transverse stress $\sigma_{33} = \nu T$ under plane strain conditions. Its magnitude is taken to be such that the material remains elastic.

The Newark-β method with $\beta = 0$ and $\gamma = 0.5$ is used to integrate the discrete equation of motion. A lumped mass matrix is chosen since it is preferred for the explicit integration procedure. A fixed time step 5×10^{-11}s is employed, which is sufficient to ensure that the numerical solutions remain stable. In the calculations, all material parameters are kept fixed to be representative of AISI 4340 steel studied experimentally by Hartley *et al*. [10]. The properties are specified by: E =200 GPa, ν =0.3, σ_0 =1250 MPa, N =0.08, m =0.01, $\dot{\varepsilon}_0$ =0.001/s, ρ =7833 kg/ m^3, $\alpha = 1.3\times10^{-5}/^0C$, $c_r = 456J/kg^0C$, $k = 54w/m^{2\,0}C$ and $\beta = 0.0016$.

RESULTS

Effects of rate dependence and thermal sensitivity in traction-separation laws

Our first attention is focused on the effects of strain rate sensitivity and thermal softening factors in the cohesive zone model. Computations are carried out for specified material properties, $\hat{\sigma}_0 = 2.5\sigma_0$ and $\dot{K}_I = 10^7 MPa\sqrt{m}/s$ for different values of r_1 and r_2. Figures 1 and 2 show the R-curves for the two cases: (i) r_1=0.01 and r_2=0.001 and (ii) r_1=0.002 and r_2=0.001. The R-curves rise steadily after only a small amount of crack growth. It is seen that strain rate sensitivity plays a beneficial role in toughness enhancement, because higher magnitudes of toughness can be obtained at r_1=0.01 than at r_1=0.002. Physically, rate effect can act effectively through an increase in energy dissipation in the plastic zone since the fracture stress is enhanced by rate sensitivity in the fracture zone.

In Fig. 3, the variation of K_{Id} is plotted against $\Delta a/R_0$ for r_2=0.003 and r_1=0.002, so that the thermal effect becomes dominant over rate dependence. It is observed that at high r_2, crack growth resistance is much reduced. However, when $\Delta a/R_0$ >0.005, the slopes of the R-curves increase to the same order as those at small r_2. This is because, as the crack advances, the thermal softening is weakened severely and strain-rate hardening prevails.

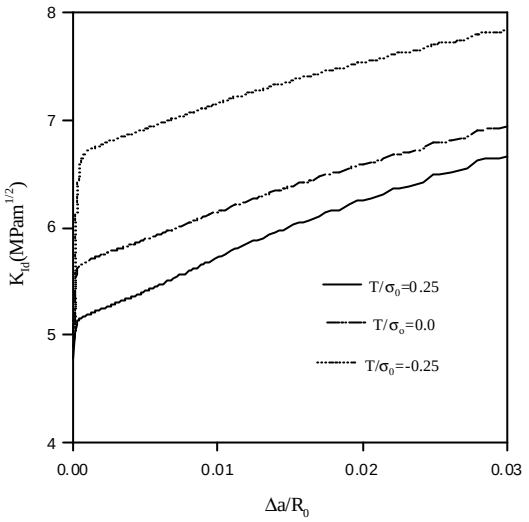

Fig. 1. Crack growth resistance curves for r_1=0.01, r_2=0.001 at three different T-stress

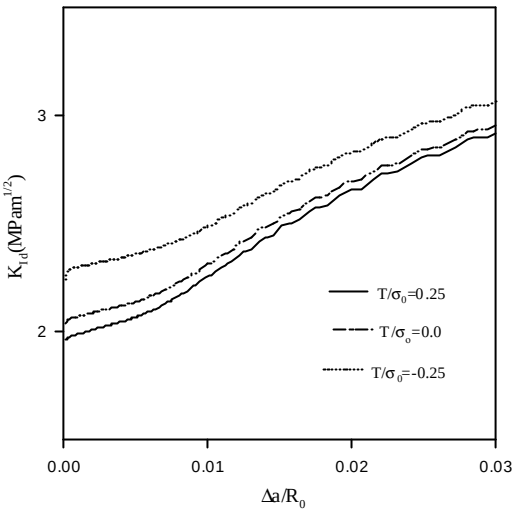

Fig. 3. Crack growth resistance curves for r_1=0.002, r_2=0.003 at three different T-stress

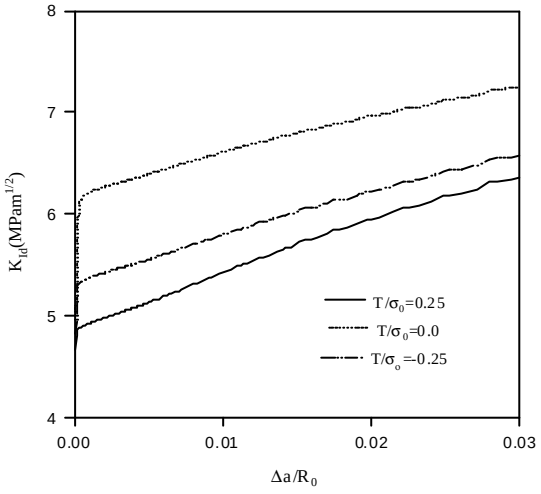

Fig. 2. Crack growth resistance curves for r_1=0.002, r_2=0.001 and $\hat{\sigma}_0$=2.5σ_0, at three different levels of T-stress and $\dot{K}_I = 10^7 MPa\sqrt{m}/s$.

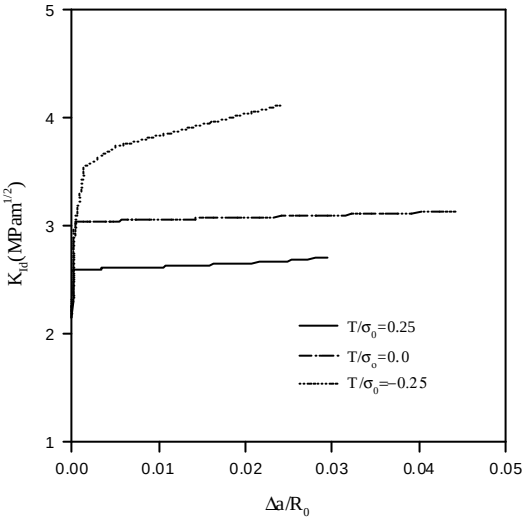

Fig. 4. Crack growth resistance curves for r_1=0.002, r_2=0.001 and $\hat{\sigma}_0$=2.5σ_0, at three different levels of T-stress and $\dot{K}_I = 10^6 MPa\sqrt{m}/s$.

Effects of loading rates

For comparison, two impact velocities $\dot{K}_I$ = 10^6 and $10^7 MPa\sqrt{m}/s$ are used with material constants r_1=0.002, r_2=0.001 and $\hat{\sigma}_0$=2.5σ_0. The R-curves at the higher impact speed are shown in Fig. 2, while those R-curves at the lower speed are shown in Fig. 4. There is a reduction in the fracture toughness with the lower impact speed. This is because high strain-rate increases the stress ahead of the crack-tip. Similarly, the fracture stress is enhanced by the rate-dependent cohesive law. Further, plastic deformation is restricted at low loading rates. The crack speed at different loading rates are examined in Figs. 2 and 4. It is found that the crack speed is larger at low impact speeds than at high impact speeds. The steady-state crack speed at $T/\sigma_0 = -0.25$ is 518m/s at the higher impact speed and 648m/s at the lower impact speed.

Effects of crack-tip constraints

Although the loss of crack-tip constraint plays an important role in the toughness enhancement of

cleavage fracture, the constraints cannot significantly affect the toughness at crack initiation for ductile fracture at low loading rates, as shown in Fig.4. The sensitivity of crack initiation toughness to T-stress can be found at high loading rates, as shown in Figs. 1 to 3. For example, the initiation toughness is 4.78 MPa $\sqrt{m}$ for T/σ_0 =0.25 and 5.03 MPa $\sqrt{m}$ for T/σ_0 =-0.25 in Fig. 1. In addition, negative T-stress can decrease crack speed during the early stage of crack growth.

Negative T-stress can increase fracture toughness significantly. There is a large difference in the R-curves between T=-0.025 and 0.25. At high loading rates, the difference in toughness mainly results from T-stress at the early stage and the trend is offset with crack advance. Upon full development of the crack speed, the slopes of the R-curves tend to be insensitive to the T-stress. (See Figs. 2 for example). This means that the steady-state crack speed is insensitive to the constraints. However, this is not the case at low impact rates. It is likely that the T-stress is still comparable to the fracture stress at lower loading rates.

CONCLUSIONS

(1) Crack initiation is suppressed as the rate-sensitivity factor r_1 in the cohesive law increases. The toughness is higher for larger r_1, irrespective of the impact speeds.
(2) Thermal softening caused by intense plastic deformation promotes ductile failure. This effect is more significant at the early stage of crack growth. After some crack extension, thermal effect at high r_2 is restricted and the R-curves increase at the same rate.
(3) Increasing the loading rate enhances the fracture toughness because the rate effect increases the flow strength and the fracture energy, as well as the kinetic energy. It is seen from Figs 2 and 4 that for low strain-hardening elastic-plastic materials, material inertia and rate sensitivity can increase the toughness by a factor of two.
(4) Fracture behavior is also strongly controlled by the constraint effect. However, it depends on the loading rate. Constraint does not change the crack initiation toughness at low loading rates, but it does at high loading rates. Importantly, change in the crack-tip constraint has no significant effect on the steady-state crack speed at high impact speeds.

ACKNOWLEDGEMENTS

We wish to thank the Australian Research Council (ARC) for the continuing support of this project. XZ was in receipt of an Overseas Postgraduate Research Award tenable at the University of Sydney and an ARC Research Scholarship funded from the project grant awarded to Y-W M.

REFERENCES

1. Tvergaard, V. and Hutchinson, J. W. (1992) *J. Mech. Phys. Solids* 40, 1377-1397.
2. Du, J., Thouless, M.D. and Yee, A. F. (2000) *Int. J. Fract*. 92, 271-285.
3. Langer, J. S. and Lobkovsky, A. E. (1998). *J. Mech. Phys. Solids* 46, 1521-1556.
4. Landis, C.M., Pardoen, T. and Hutchinson, J.W. (2000*) Mech. Mater*. 32, 663-678.
5. Hancock, J. W. Reuter, W. G. and Parks, D. M. (1993) In *Constraint Effects in Fracture*, ASTM STP 1171, American Society for Testing and Materials, Philadelphia, 21-40.
6. O'Dowd, P. and Shih, C. F. (1991) *J. Mech. Phys. Solids* 40, 989-1015.
7. Xia, L., Shih, C. F. (1995) *J. Mech. Phys. Solids* 43, 233-259.
8. McMeeking , R. M. and Rice, J. R. (1975) *Int. J. Solid Structures*, 11, 606-616.
9. Gao, X., Shih, C. F., Tvergaard, A. and Needleman, A. (1996) *J. Mech. Phys. Solids* 44, 1255-1282
10. Hartley, K. A., Duffy, J. and Hawley, R. H. (1987) *J. Mech. Phys. Solids* 35, 283-301.